A&A 476, 301–306 (2007)
DOI: 10.1051/0004-6361:20078444

Astronomy & Astrophysics

X-ray eclipse time delays in 4U 2129+47

E. Bozzo[1,2], M. Falanga[3], A. Papitto[1,2], L. Stella[1], R. Perna[4], D. Lazzati[4], G. Israel[1], S. Campana[5], V. Mangano[6], T. Di Salvo[7], and L. Burderi[8]

[1] INAF – Osservatorio Astronomico di Roma, Via Frascati 33, 00044 Rome, Italy
e-mail: bozzo@oa-roma.inaf.it
[2] Dipartimento di Fisica – Università di Roma Tor Vergata, via della Ricerca Scientifica 1, 00133 Rome, Italy
[3] CEA Saclay, DSM/DAPNIA/Service d'Astrophysique (CNRS FRE 2591), 91191 Gif-sur-Yvette, France
[4] JILA, University of Colorado, Boulder, CO 80309-0440, USA
[5] INAF Osservatorio Astronomico di Brera, via Emilio Bianchi 46, 23807 Merate (LC), Italy
[6] INAF Istituto di Astrofisica Spaziale e Fisica Cosmica Sezione di Palermo, via Ugo La Malfa 153, 90146 Palermo, Italy
[7] Dipartimento di Scienze Fisiche ed Astronomiche, Università di Palermo, via Archirafi 36, 90123 Palermo, Italy
[8] Università degli Studi di Cagliari, Dipartimento di Fisica, SP Monserrato-Sestu, KM 0.7, 09042 Monserrato, Italy

Received 8 August 2007 / Accepted 10 September 2007

ABSTRACT

Aims. 4U 2129+47 was discovered in the early 80's and classified as an accretion disk corona source due to its broad and partial X-ray eclipses. The 5.24 h binary orbital period was inferred from the X-ray and optical light curve modulation, implying a late K or M spectral type companion star. The source entered a low state in 1983, during which the optical modulation disappeared and an F8 IV star was revealed, suggesting that 4U 2129+47 might be part of a triple system. The nature of 4U 2129+47 has since been investigated, but no definitive conclusion has been reached.
Methods. Here, we present timing and spectral analyses of two *XMM-Newton* observations of this source, carried out in May and June, 2005.
Results. We find evidence for a delay between two mid-eclipse epochs measured ∼22 days apart, and we show that this delay can be naturally explained as being due to the orbital motion of the binary 4U 2129+47 around the center of mass of a triple system. This result thus provides further support in favor of the triple nature of 4U 2129+47.

Key words. accretion, accretion disks – binaries: eclipsing – stars: individual: 4U 2129+47 – stars: neutron – X-rays: stars

1. Introduction

4U 2129+47 was discovered by Forman et al. (1978) at a flux level variable between 2.4 and 4.8×10^{-10} erg cm^{-2} s^{-1} (2−10 keV band). Observations of 4U 2129+47 in the early 80's showed that both its X-ray and optical light curves were modulated over a 5.24 h period, with a partial V-shaped minimum maintaining approximately the same shape and phase (Thorstensen et al. 1979; Ulmer et al. 1980; McClintock et al. 1982, hereafter MC82). A late K or M spectral type companion of ∼0.6 $M_{\odot}$ was suggested, assuming it filled its Roche lobe, and the discovery of a type I X-ray burst (Garcia & Grindlay 1987) led to the classification of 4U 2129+47 as a neutron star (NS) low mass X-ray binary (LMXB) system (Thorstensen et al. 1979; McClintock et al. 1981; MC82). The source distance was estimated to be ∼1−2 kpc, corresponding to an X-ray luminosity of $\sim 5 \times 10^{34}$ erg s^{-1} (Horne et al. 1986). The optical light curve could be understood in terms of the varying viewing geometry of the X-ray heated face of the companion, while the V-shaped minimum in the X-ray light curve was interpreted as being due to the gradual eclipse of an extended accretion disk corona (ADC). The shape of the partial X-ray eclipse and the rapidity of its ingress and egress have been used to place upper limits on the size of this X-ray scattering region ($\sim 5 \times 10^{10}$ cm for the 4U 2129+47 high luminosity state, MC82). The origin of ADCs is not well understood yet, but it is most likely related to systems in which the mass accretion rate is sufficiently high that a tenuous scattering corona is formed as a consequence of matter evaporation from the accretion disk (White & Holt 1982).

4U 2129+47 was first revealed in a low state ($F_{0.3-6\ \mathrm{keV}} \lesssim 10^{-12}$ erg cm^{-2} s^{-1}) in September 1983 (Pietsch et al. 1986; Wenzel et al. 1983). Optical observations carried out between 1983 and 1987 showed a flat light curve without any evidence for orbital modulation, while the spectrum displayed features fully compatible with a late type F8 IV star (Kaluzny 1988; Chevalier et al. 1989). The hypothesis of a foreground or a background star seemed unlikely, due to the low probability ($\lesssim 10^{-3}$) of chance superposition. This led to the suggestion that 4U 2129+47 is part of a triple system (Thorstensen et al. 1988). The revised estimate of the source distance was ∼6.3 kpc (Cowley & Schmidtke 1990; Deutsch et al. 1996).

Hints of a possible detection of a dynamical interaction between the F star and 4U 2129+47 were discussed by Garcia et al. (1989) and Cowley & Schmidtke (1990), after the discovery of a ∼40 km s^{-1} shift in the mean radial velocity measurement derived from the F star spectrum. Shifts of this amplitude are indeed expected if the F star is in a month-long orbit around the binary (Garcia et al. 1989).

ROSAT and *Chandra* observations, carried out between 1991 and 2000, led to a characterization of the low luminosity state of 4U 2129+47 (Garcia et al. 1992; Garcia 1994; Garcia & Callanan 1999). The refined *Chandra* position turned out to be coincident with the F star to within 0.″1 (Nowak et al. 2002,

hereafter N02) providing support in favor of the triple nature of 4U 2129+47. However, a firm conclusion could not be reached.

Here we report on *XMM-Newton* observations of 4U 2129+47, and discuss the likely detection of a mid-eclipse epoch variation between two ∼22 days distant observations. We show that this delay is naturally explained as being due to the orbital motion of the binary 4U 2129+47 with respect to the center of mass of a triple system. This delay is thus probably the first "Doppler" (or, more accurately, "Roemer") X-ray signature of the triple nature of 4U 2129+47. We outline our data reduction procedure in Sect. 2, and present the results of timing and spectral analysis in Sect. 3. Our conclusions are summarized in Sect. 4.

2. Observations and data

XMM-Newton (Jansen et al. 2001) observed 4U 2129+47 on May 15 and on June 6, 2005 for a total time span of ∼80 ks (about four orbital periods). The total effective exposure time for each observation was ∼13 ks for the EPIC-PN, EPIC-MOS1, and EPIC-MOS2 cameras. The remaining observing time was discarded due to ground station anomalies and high radiation from solar activity filling up of the EPIC-PN scientific buffer. Heavy contamination due to solar activity resulted in poor orbital phase coverage, especially during the first observation. Furthermore, the EPIC-PN and EPIC-MOS cameras were found to be unequally affected by this contamination, thus forcing a different selection of good time intervals for the spectral and timing analyses (see Sect. 3). The observation data files (ODFs) were processed to produce calibrated event lists using the standard *XMM-Newton* Science Analysis System (SAS 7.0). We used the EPCHAIN and EMCHAIN tasks for the EPIC-PN and the two MOS cameras, respectively. Source light curves and spectra were extracted in the 0.2−10 keV band, using circles of ∼14.6″ radius centered on the source. This corresponds to ∼70% encircled energy[1] for both the EPIC-PN and EPIC-MOS cameras. Larger circles could not be used due to the proximity of the S3–β Digital Sky Survey stellar object (N02). We extracted the background light curves and spectra from circles of radii ∼116″ in the nearest source-free region to 4U 2129+47. Background and source circles were all chosen to lie within the same CCD. The difference in extraction areas between source and background was accounted for by using the SAS BACKSCALE task for the spectra and the LCMATH task from HEASOFT (version 6.1.1) for the light curves. The average source count rate was found to be 0.041 ± 0.001 count s^{-1} in the EPIC-PN and 0.010 ± 0.001 count s^{-1} in the two EPIC-MOS cameras (errors are 1σ). Given the short effective exposure time, the low count rate of the EPIC-MOS1 and EPIC-MOS2 cameras did not contribute significantly to the spectral analysis; therefore in Sect. 3.2 we discuss only the spectrum from the EPIC-PN camera.

3. Results

3.1. Orbital ephemerides and eclipse parameters

In the *XMM-Newton* EPIC-PN light curves, two eclipses were clearly detected, one in each pointing. These eclipses were also unambiguously found in the EPIC-MOS1 and EPIC-MOS2 data. In order to avoid any non-synchronicity problems between the three EPIC cameras, we followed method III of Barnard et al. (2006). In accordance with this method, all the source and background time series of the same observation were extracted within the time interval around the eclipse that was found not to be interrupted by the presence of a previously removed solar flare (Sect. 2). In all cases, the time interval selection was carried out by filtering each light curve with the EVSELECT (version 3.59) keywords "timemin" and "timemax". This additional reduction of the effective exposure time (in addition to the one described in Sect. 2) was especially restrictive for the first observation, for which a total exposure time of only ∼4 ks around the eclipse could be used. The times of all light curves were corrected to the barycentre of the Solar System with the SAS BARYCEN task (version 1.17.3), and summed up in each observation with the LCMATH task, in order to maximize statistics and thus improve the accuracy with which the eclipse parameters could be determined. To estimate the mid-eclipse times, the light curves were rebinned in 300 s bins[2].

These light curves were then fit with a rectangular eclipse model, in which the mean count-rate outside ($F_{\rm max}$) and inside ($F_{\rm min}$) eclipse, and the mid-eclipse epoch (T_0), were treated as free parameters. In these fits we fixed the duration of the eclipse at the value 1523 s, as measured by N02. Being dictated by the secondary star, the duration of the eclipse limb is unlikely to have changed since the time of the *Chandra* observation (see Sect. 3.2 for details). χ^2 minimization was performed with an IDL routine written by the authors. The model rectangular eclipse was integrated over each time bin before the χ^2 was computed, in order to take data binning into account[3]. With this method we obtained an accurate determination of the eclipse mid-epoch, even though the ingress and egress eclipse times could not be determined with the same accuracy. The χ^2 hyper-surface was directly sampled in a fine grid of values in order to distinguish local minima. The variance between model and data was then calculated in each point and for each set of parameters, in order to investigate the local χ^2 minima in the 4D parameter space. The best fits to the eclipse epochs were found to be T_0(a) = 2 453 506.4825 ± 0.0003 JD and T_0(b) = 2 453 528.3061 ± 0.0004 JD with χ^2/d.o.f.(a) = 9/11, χ^2/d.o.f.(b) = 44/42 (errors are at 68% confidence level unless otherwise specified; our epochs are given in UT[4]). The values of the reduced χ^2 in the above fits are close to 1 and therefore the addition of any other free parameter in the fit would not be justified from a statistical point of view. We also checked that by allowing the eclipse duration to vary within the N02's 1σ confidence level, i.e., 1473−1553 s, the other parameters of the best fit remain unchanged to within the errors (mid-eclipse epochs differed by less than 10 s and the 1σ errors remained below 26 s). We note however that if the eclipse duration is included as a free parameter without any constrains, a less significant eclipse delay of $\delta T_{\rm m}$ = 151 ± 55 s would be obtained.

[1] As described in chapter 3.2.1.1 (Issue 2.5) of the *XMM-Newton* users' handbook.

[2] A check was carried out a posteriori to verify that our results are virtually independent of the light binning time.

[3] Standard fitting routines that compute the fitting function punctually in the center of the bin are not adequate when a function with a large first derivative or features with a scale smaller than the bin time is considered. In our case the derivative diverges at the ingress and egress times.

[4] Note that HJD(UT) = HJD(TT) − 64.68 s at our epochs. We did not consider the correction for the difference between heliocentric Julian date in the geocentric (terrestrial) dynamical time system, HJD(TT), and barycentric dynamical time system, BJD(TB). The latter is the one used by the SAS BARYCEN task, but the difference between BJD(TB) and HJD(TT) is less than ∼3 s at any given time, which is much smaller than the accuracy of our measurement here.

Table 1. Mid-eclipse epoch measurements.

Observatory	Mid-eclipse Epoch[a] (JD)	Orbital Period[a] (s)	References
HEAO 1 and *Lick Observatory telescope*	2 443 760.755(3)	18 857(3)	Thorstensen et al. (1979) (Th79)
McGraw Hill telescope and *KPNO telescope*	2 444 107.785(3)	18 857.5(1)	McClintock et al. (1981) (MC81)
Einstein	2 444 403.743(2)	18 857.48(7)	McClintock et al. (1982) (MC82)
Louisiana State Telescope, *McGraw Hill telescope*			
Chandra	2 451 879.5713(2)	18 857.631(5)[b]	Nowak et al. (2002) (N02)
XMM-Newton	2 453 506.4825(3)	18 857.594(7)	this work (tw)
XMM-Newton	2 453 528.3061(4)	–	this work (tw)

[a] Numbers in parentheses are the uncertainties on the last significant digit (errors at 1σ level).
[b] Average orbital period calculated by using the two *Chandra* eclipses.

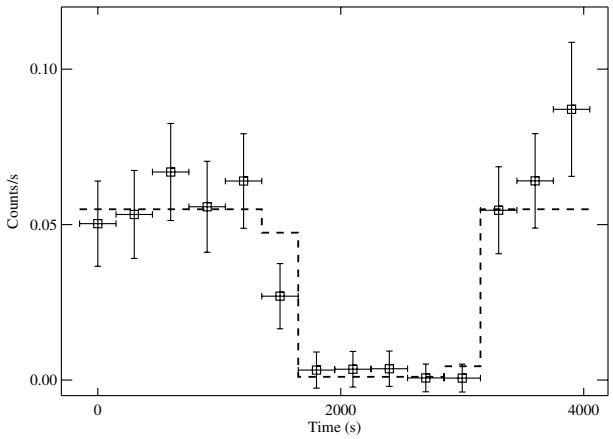

Fig. 1. Fit of the mid-eclipse epoch during the first observation. The 0.2−10 keV light curve (bin time 300 s) is shown together with the best fit model (dashed line).

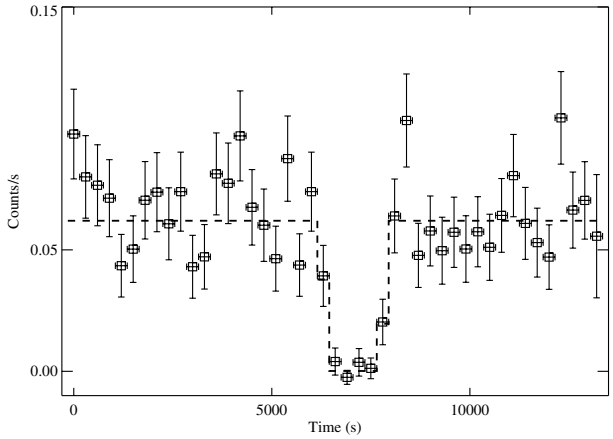

Fig. 2. Fit of the mid-eclipse epoch during the second observation. The 0.2−10 keV light curve (bin time 300 s) is shown together with the best fit model (dashed line).

In the following we adopt values of the two mid-eclipse epochs as derived from the first fit. We show in Figs. 1 and 2 the two eclipses, together with the best fit models discussed above. We also carried out the fits by using a modified version of the eclipse model by Mangano et al. (2004) in order to estimate the eclipse ingress and egress time. We allowed these times to take independent values during the fit (N02). Only upper limits of $\lesssim$310 s could be derived, which are significantly larger than those obtained from the *Chandra* observation (in 130−260 s range, N02).

In order to determine a refined orbital solution, we considered the above mid-eclipse epochs together with the epochs, T_n, derived from earlier observations (see Table 1). As discussed in Sect. 1, the observed phase alignment between the X-ray and optical light curve minima, allows the comparison of optical and X-ray measurements of the system's ephemerides. The long time span covered by the eclipse measurements (1979−2005 or $n_{\rm max} \sim 44\,800$) can be used to improve the accuracy of the orbital solution and, possibly, measure the orbital period derivative. To this aim we used a standard O–C technique[5]. We considered the ephemeris from MC82 as reference ($T_{\rm ref} = 2\,444\,403.743 \pm 0.002$ JD, $P_{\rm ref} = 18\,857.48 \pm 0.07$ s), and plotted in Fig. 3 the delays $\Delta T_n = T_n - T_{n_{\rm pred}}$. Here $T_{n_{\rm pred}} = T_{\rm ref} + nP_{\rm ref}$, with n the closest integer to $(T_n - T_{\rm ref})/P_{\rm ref}$ (our two observations correspond to $n = 41\,706$, $41\,806$). In the same figure we have also plotted the best quadratic fit to the O−C residuals, corresponding to an orbital period evolution with constant time derivative. A linear fit (i.e., a constant orbital period) to the same data gave an unacceptable fit (χ^2/d.o.f. = 91/4). Table 2 gives our corrected reference time, $T_{\rm ref}$, orbital period, $P_{\rm ref}$, and the derived orbital period evolution $P_{\rm orb}\dot{P}_{\rm orb}^{-1} = (5.8 \pm 0.7) \times 10^6$ yr. This value is a factor of ∼4 larger than that in N02, but we note that N02's estimate was deduced by adopting the MC82 value of $P_{\rm orb}$ and accounting for the entire measured delay as being due to an orbital period derivative. The observed delay of ∼6500 s between the ephemeris of MC82 and the one found in the present work (see Fig. 3), implies an orbital phase shift of ∼0.35. Small deviations in the eclipse centroid between the active and quiescent state of 4U 2129+47 may be introduced by changes in the shape of the ADC around the compact object. However a ∼6500 s delay is far too large to be explained as a result of such geometrical variations. The poor χ^2 in Table 2 is due to the large shift of the first *XMM-Newton* point with respect to the second one ($\delta T_{\rm m} = 192 \pm 43$ s), which could not be accounted for by any quadratic fit to the eclipse phase evolution. While this delay is much smaller than that discussed above, we argue that it is also very unlikely to result from geometrical variations within the 4U 2129+47 binary system. This is because the eclipse profile is consistent with the central source being eclipsed by the companion star. Moreover, the source X-ray flux and spectrum remained virtually the same across the two *XMM-Newton* observations and the *Chandra* observation discussed by N02 (see Sect. 3.2). In Sect. 4 we discuss the possibility that this delay is due to light propagation in a triple system.

[5] Observed minus calculated residuals, which are the delay in eclipse time over that expected for a constant period system (see, e.g., Parmar et al. 1991; Papitto et al. 2005, and references therein).

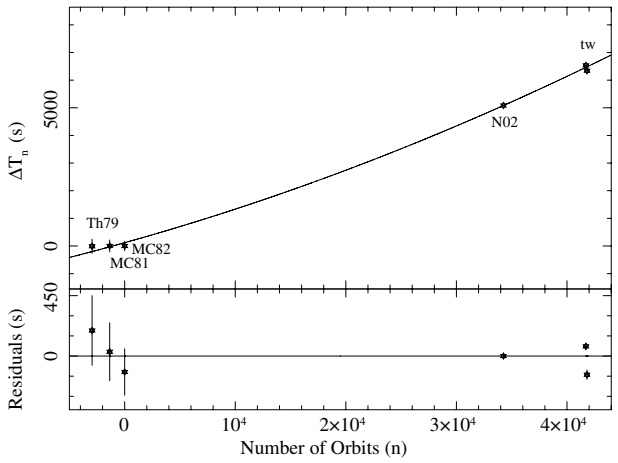

Fig. 3. Delays of the mid-eclipse epochs with respect to a constant $P_{\rm orb} = P_{\rm ref}$ model. The solid line in the upper panel represents the quadratic best fit to the epochs (see Sect. 3.1). The lower panel shows the residuals from this fit.

Table 2. Orbital solution obtained with the best quadratic fit to the O−C delays ΔT_n (see Fig. 3).

$T_{\rm ref}$ (JD)	$2\,444\,403.7443 \pm 0.0013$
$P_{\rm orb}$ (s)	$18\,857.594 \pm 0.007$
$\dot{P}_{\rm orb}$ (s s^{-1})	$(1.03 \pm 0.13) \times 10^{-10}$
$P_{\rm orb}\dot{P}_{\rm orb}^{-1}$ (yr)	$(5.8 \pm 0.7) \times 10^6$
χ^2/d.o.f.	25.6/3

We also extracted the EPIC-PN light curves of the observations, since these have a better orbital phase coverage than those obtained by summing all three instruments. This however resulted in a lower count rate and S/N. These light curves and those obtained by using data summed over the three EPIC cameras were folded at the best orbital solution using 10 phase bins. We fitted these two light curves with the function $F(\phi) = A + B\sin[2\pi(\phi - \phi_0)]$, and looked for a sinusoidal modulation similar to that observed by N02. No significant modulation was observed (fitting with a constant value gave a χ^2/d.o.f. of 12/13 and 10/17 respectively). We derived a 90% confidence upper limit on the amplitude modulation of ∼17%, i.e., a factor of ∼2 smaller than the value reported by N02. This result was also checked by using light curves extracted only in the 0.5−2.0 keV band, where the amplitude modulation might be higher (N02). No significant differences were found. We discuss these results in Sect. 4, together with the results from the spectral analysis (Sect. 3.2).

3.2. Spectral analysis

Spectral analysis was carried out by using XSPEC version 11.3.2t (Arnaud 1996); the data were rebinned in order to have at least 20 photons in each energy bin. Owing to poor statistics, phase-resolved spectroscopy could not be carried out. Instead, the spectra of the two observations were accumulated during the same time intervals selected for the extraction of the EPIC-PN light curves, except for the eclipses (see Sect. 3.1).

The spectrum of the first observation was modeled with only an absorbed blackbody (poor statistics did not allow for more complex models).

The second observation was first modeled with an absorbed power law plus a blackbody component, but the F-statistics probability with respect to a simple absorbed blackbody model was found to be ∼0.2. The best fit was then obtained, also in this case, by adopting an absorbed blackbody model.

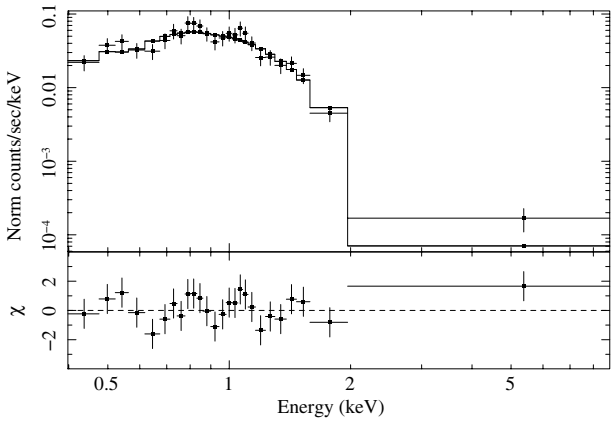

Fig. 4. Measured 0.2−10 keV spectrum of 4U 2129+47 during the second pointing. The best fit model and the contribution of the fit residuals to the χ^2 are also shown.

A power law component with fixed photon index $\Gamma = 1.1$ (N02) was added to the fit of the second observation in order to estimate an upper limit. For such a power law component, the 90% confidence upper limit was about 10% of the 0.2−10 keV unabsorbed flux (in agreement with N02, see their model A). C-statistics model fitting (Cash 1979) was also performed on the unbinned spectra: the results were fully compatible with those obtained by using χ^2 minimization. Figure 4 shows the spectrum and model of the second pointing as an example, while the best fit parameters are reported in Table 3. No significant difference was found between the two *XMM-Newton* observations, and all parameters were compatible, to within the errors, with those determined by N02 for the quiescent state of 4U 2129+47. We also tested our results with the XSPEC NSA model (Arnaud 1996; Zavlin et al. 1996). Fits were carried out, first by using a fixed distance of 6.3 kpc, and then by fixing a neutron star radius of 5 and 10 km (N02). Results of these fits were found to agree with those of N02 (our errors on all parameters are a factor of ∼1.5 larger).

4. Discussion

We reported on *XMM-Newton* observations of 4U 2129+47 in its quiescent state, which has lasted, apparently uninterrupted, since 1983 (Wenzel et al. 1983). The discovery of a late F-type star coincident with the position of 4U 2129+47 (Thorstensen et al. 1988; Chevalier et al. 1989) led to the hypothesis that this binary system might be part of a hierarchical triple. Our detection of a delay $\delta T_{\rm m} = 192 \pm 43$ s across two eclipses separated by ∼22 days, can be naturally explained as being due to the orbital motion of the binary with respect to the center of mass of a triple, and thus lends support in favor of the triple system hypothesis.

Using a third star of mass M_1, an inner binary with $M_2 \sim 2\ M_\odot$, and a non-eccentric orbit, the expected delay between two mid-eclipse epochs separated by a time interval τ can be expressed as

$$\delta T = a_2 \sin i/c\,[\sin(\phi_0 + \delta\phi) - \sin\phi_0]\,. \quad (1)$$

Here $a_2 = (G/4\pi^2)^{1/3} P_{\rm tr}^{2/3} M_1/(M_1 + M_2)^{2/3}$ is the radius of the inner binary orbit around the triple system center of mass (with

Table 3. Best-fit spectral parameters with $N_{\rm H}$ and BB model (90% confidence level error bars).

	1 Obs. (May-15-2005)		2 Obs. (June-6-2005)	
	χ^2-Stat	C-Stat	χ^2-Stat	C-Stat
$N_{\rm H}$ (10^{22} cm^{-2})	$0.14^{+0.11}_{-0.09}$	$0.24^{+0.03}_{-0.09}$	$0.21^{+0.1}_{-0.06}$	$0.28^{+0.03}_{-0.08}$
$kT_{\rm bb}$ (keV)	$0.25^{+0.03}_{-0.03}$	$0.22^{+0.03}_{-0.02}$	$0.20^{+0.02}_{-0.02}$	$0.18^{+0.02}_{-0.01}$
$R^{\rm a}_{\rm bb}$ (km)	$1.3^{+1.1}_{-0.4}$	$1.9^{+0.74}_{-0.53}$	$2.42^{+1.8}_{-0.7}$	$2.87^{+1.7}_{-0.6}$
χ^2/d.o.f.	14.30/14	–	20.6/23	–
C-Stat	–	496.8	–	592.24
$F^{\rm a}_{0.2-10\ {\rm keV}}$ (10^{-14} erg cm^{-2} s^{-1})	9.3	9.3	8.9	9.0
$F^{\rm b}_{0.2-10\ {\rm keV}}$ (10^{-13} erg cm^{-2} s^{-1})	1.6	2.3	2.2	3.3
$L^{\rm c}_{0.2-10\ {\rm keV}}$ (10^{32} erg s^{-1})	7.7	10.9	10.5	15.8

[a] Absorbed flux.
[b] Unabsorbed flux.
[c] From the unabsorbed flux and assuming a distance of 6.3 kpc.

a period $P_{\rm tr}$), ϕ_0 is the phase at T_0(a) of the binary system along such an orbit, c is the speed of light, i is the inclination angle of the triple system orbit, $\delta\phi = 2\pi\tau P_{\rm tr}^{-1}$ and, in our case, $\tau = T_0({\rm b}) - T_0({\rm a}) \simeq 22$ d.

Figure 5 shows a plot of the range of allowed values of the triple orbital period as a function of the third star mass[6], which give delays compatible with the measured value $\delta T_{\rm m}$ (to within the uncertainties at a given confidence level). The dashed, dot-dashed and dot-dot-dot-dashed lines represent the ranges for $1\sigma = 43$ s, $2\sigma = 85$ s and $3\sigma = 165$ s confidence intervals in $\delta T_{\rm m}$, respectively. The solid lines give the constraints on $P_{\rm tr}$ imposed by the measured ~40 km s^{-1} shift in the mean radial velocity of the F star (Garcia et al. 1989), under the assumption that this represents the maximum observable radial velocity shift of its orbit. The two panels of Fig. 5 show the cases of $i = 90°$, and $i = 60°$ respectively. From the upper panel of this figure ($i = 90°$) it can be seen that, at 1σ confidence level, we can set a lower limit on the F star mass of ~1.2 $M_\odot$. Considering a 2σ uncertainty on $\delta T_{\rm m}$ removes the upper limit on M_1 and only the orbital period can be constrained (39 d $< P_{\rm tr} <$ 200 d, for $M_1 \simeq 1\ M_\odot$). We note that a decrease of the inclination angle results in a smaller range of allowed orbital periods, while the effect of a non-zero eccentricity (hypothesis not considered in our calculation) would have the opposite effect.

The possibility that 4U 2129+47 is in a triple system might also have noticeable consequences for our measured orbital period derivative, $P_{\rm orb}\dot{P}^{-1}_{\rm orb} = (5.8 \pm 0.7) \times 10^6$ yr (see Sect. 3.1). At first sight, this value seems to imply that, as in other known LMXBs (e.g., X 1822-371, Parmar et al. 2000; Heinz & Nowak 2001; White et al. 1995) the orbital period of 4U 2129+47 is increasing. This would be contrary to evolutionary expectations. In fact, angular momentum losses (such as gravitational wave emission and magnetic breaking) in a binary system with an orbital period of ~5 h and a non-degenerate companion would imply a decreasing orbital period (Verbunt 1993). However, if a modulation in the eclipse arrival time of amplitude $T_{\rm a} = a_2 \sin i/c$ (as discussed above) contributes to the measured epochs of the eclipses, caution should be used with any estimate of $P_{\rm orb}\dot{P}^{-1}_{\rm orb}$ (such as that in Sect. 3.1) that does not take this modulation into account. Given our poor knowledge of the parameters of the triple system, a detailed correction for the orbital motion of the inner binary around the center of mass of the triple cannot be carried out yet. A conservative estimate of $P_{\rm orb}\dot{P}^{-1}_{\rm orb}$ can be derived by increasing the uncertainties on the observed ΔT_n up to a value $T_{\rm a}$, which represents the unknown amplitude of the modulation in the eclipse arrival times. The range of values that $T_{\rm a}$ may attain depends mainly on the range of orbital periods for which a solution of Eq. (1), compatible with the values of τ and $\delta T_{\rm m}$ we measured, exists. Unfortunately, the range on $P_{\rm tr}$ that can be inferred from Fig. 5 is fairly loose. Based on our 1σ range of $\delta T_{\rm m}$, we derive a minimum upper limit of $P^{\rm upp}_{\rm tr} \simeq 75$ d for the third star orbital period (for $M_1 \simeq 1.2\ M_\odot$ and $i = 90°$), which corresponds to $T_{\rm a} \simeq 100$ s. We checked that increasing the uncertainty on the measured values of the eclipse epochs by this value would remove entirely the need to introduce an orbital period derivative. By analogy we speculate that the presence of a third body in a wide orbit around the inner binary might explain the positive orbital period derivative observed in some LMXBs, which is at odds with the expectations of the standard evolutionary scenario.

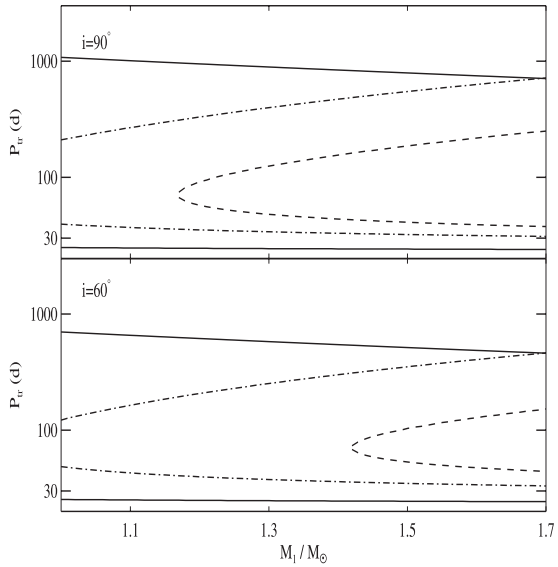

Fig. 5. Allowed regions of the triple orbital period, $P_{\rm tr}$, as a function of the third star mass, M_1, in the cases in which the measured delay $\delta T_{\rm m} = 192$ s is varied within 1σ (dashed line), 2σ (dot-dashed line) and 3σ (dot-dot-dot-dashed line) confidence level. For the 3σ range only the lower limit is drawn. Solid lines represent the limits imposed by the measured radial velocity shifts of the F-star (see text for more details). The two panels show the cases $i = 90°$ and $60°$.

Due to the low count-rate, and short effective exposure time, our *XMM-Newton* observations did not detect any spectral

[6] For an F-type star it is expected $M_1 \sim 1$–$1.6\ M_\odot$ (see, e.g., Bohm-Vitense 1992).

component above 2 keV. An absorbed ($N_{\rm H} \sim 0.2 \times 10^{22}$ cm^{-2}) blackbody component with $kT_{\rm bb} \sim 0.2$ keV and $R_{\rm bb} \sim 2$ km provided an adequate modeling of the spectrum.

For quiescent NSs in LMXBs, like 4U 2129+47, this soft X-ray emission can be produced in several alternative ways. One possibility is that this emission is powered by thermal energy released as the NS cools in between accretion phases (Brown et al. 1998; Colpi et al. 2001; Wijnands 2002). Alternative models invoke a NS in the propeller regime, shock emission due to the interaction between the pulsar wind and matter in the vicinity of the companion star, and residual accretion onto the compact star (see, e.g., Stella et al. 1994; Campana et al. 1998). While the properties of the propeller regime are still rather uncertain, a power law emission of photon index 1−2 should be expected at least in the last two interpretations (Campana et al. 1998; N02). Discriminating between these models is not possible based on our results, given the lack of information at energies above 2 keV.

A soft spectral component with similar properties, plus a power law component with photon index ∼1.1, was observed in the quiescent state of 4U 2129+47 in December 2000 (N02). However, also this observation was hampered by a low number of counts above 2 keV, thus preventing an accurate characterization of the power law emission. Some indication was found that the power law component was consistent with being of constant amplitude and slope, while the blackbody component was sinusoidally modulated over the orbital period, in a manner consistent with neutral column density variation (a factor of ∼2). This modulation was ascribed to the presence of a vertically extended disk atmosphere, thicker at the outer rim, close to the region where the accretion stream from the secondary star impacts.

As discussed in Sect. 3.2, our folded light curve showed no clear indication of a sinusoidal modulation. The upper limit we derived on the amplitude of this modulation is significantly lower than that discussed by N02 (a factor of ∼2). This suggests that there has been some change in the geometry of the outer disk region (in particular the region where the stream from the secondary impacts) across the *Chandra* and *XMM-Newton* observations.

A series of monthly spaced *XMM-Newton* or *Chandra* observations would afford a much more accurate characterization of the quiescent emission of 4U 2129+47 and measure with good accuracy the modulation in the X-ray eclipse times due to the third body. This will yield much needed information on the triple system parameters and single out unambiguously any orbital period evolution.

Acknowledgements. EB thanks University of Colorado at Boulder and JILA for the hospitality during part of this work, E. Piconcelli, E. Costantini and N. Rea for useful discussions. MF acknowledges the French Space Agency (CNES) for financial support. This work was partially supported through ASI and MIUR grants.

References

Arnaud, K. A. 1996, ASPC, 101, 17
Barnard, R., Trudolyubov, S., Haswell, C. A., et al. 2007, A&A, 469, 875
Bohm-Vitense, E. 1992, Introduction to stellar astrophysics (Cambridge University press)
Brown, E. F., Bildsten, L., & Rutledge, R. E. 1998, ApJ, 504, L95
Campana, S., Colpi, M., Mereghetti, S., Stella, L., & Tavani, M. 1998, A&ARv, 8, 279
Cash, W. 1979, ApJ, 228, 939
Chevalier, C., Ilovaisky, S. A., Motch, C., Pakull, M., & Mouchet, M. 1989, A&A, 217, 108
Colpi, M., Geppert, U., Page, D., & Possenti, A. 2001, ApJ, 548, L175
Cowley, A. P., & Schmidtke, P. C. 1990, ApJ, 99, 678
Deutsch, E. W., Margon, B., Wachter, S., & Anderson, S. F. 1996, ApJ, 471, 979
Forman, W., Jones, C., Cominsky, L., et al. 1978, ApJ, 38, 357
Garcia, M., Grindlay, J., & Bailyn, C. 1992, IAUC, 5578, 2
Garcia, M. R. 1994, ApJ, 435, 407
Garcia, M. R., & Callanan, P. J. 1999, ApJ, 118, 1390
Garcia, M. R., & Grindlay, J. E. 1987, ApJ, 313, L59
Garcia, M. R., Bailyn, C. D., Grindlay, J. E., & Molnar, L. A. 1989, ApJ, 341, L75
Heinz, S., & Nowak, M. A. 2001, MNRAS, 320, 249
Horne, K., Verbunt, F., & Schneider, D. P. 1986, MNRAS, 218, 63
Jansen, A., Lumb, D., Altieri, B., et al. 2001, A&A, 365, L1
Kaluzny, J. 1988, Acta Astron., 38, 207
Mangano, V., Israel, G. L., & Stella, L. 2004, A&A, 419, 1045
McClintock, J. E., Remillard, R. A., & Margon, B. 1981, ApJ, 243, 900 (MC81)
McClintock, J. E., London, R. A., Bond, H. E., & Grauer, A. D. 1982, ApJ, 258, 245 (MC82)
Nowak, M. A., Heinz, S., & Begelman, M. C. 2002, ApJ, 573, 778 (N02)
Papitto, A., Menna, M. T., Burderi, L., et al. 2005, ApJ, 621, L113
Parmar, A. N., Smale, A. P., Verbunt, F., & Corbet, R. H. D. 1991, ApJ, 366, 253
Parmar, A. N., Oosterbroek, T., Del Sordo, S., et al. 2000, A&A, 356, 175
Pietsch, W., Steinle, H., Gottwald, M., & Graser, U. 1986, A&A, 157, 23
Stella, L., Campana, S., Colpi, M., Mereghetti, S., & Tavani, M. 1994, ApJ, 423, L47
Thorstensen, J., Charles, P., Bowyer, S., et al. 1979, ApJ, 233, L57 (Th79)
Thorstensen, J. R., Brownsberger, K. R., Mook, D. E., et al. 1988, ApJ, 334, 430
Ulmer, M. P., Shulman, S., Yentis, D., et al. 1980, ApJ, 235, L159
Verbunt, F. 1993, ARA&A, 31, 93
Wenzel, W. 1983, IBVS, 2452, 1
White, N. E., & Holt, S. S. 1982, ApJ, 257, 318
White, N. E., Nagase, F., & Parmar, A. N. 1995, X-ray Binaries, ed. W. H. G. Lewin, J. Van Paradijs, & E. P. J. van den Heuvel (Cambridge University Press)
Wijnands, R. 2002, ASPC, 262, 235
Zavlin, V. E., Pavlov, G. G., & Shibanov, Y. A. 1996, A&A, 315, 141